Behavior of Hydroxide at the Water/Vapor Interface

Bernd Winter,[1*] Manfred Faubel,[2] Robert Vácha,[3] and Pavel Jungwirth[3*]

[1]Helmholtz-Zentrum Berlin für Materialien und Energie and BESSY, Albert-Einstein-Strasse 15, D-12489 Berlin, Germany, *[2]Max-Planck-Institut für Dynamik und Selbstorganisation, Bunsenstrasse 10, D-37077 Göttingen, Germany,* *[3]Institute of Organic Chemistry and Biochemistry, Academy of Sciences of the Czech Republic and Center for Complex Molecular Systems and Biomolecules, Flemingovo nám. 2, 16610 Prague 6, Czech Republic,*

Abstract

Hydroxide and hydronium, which represent the ionic products of water autolysis, exhibit a peculiar surface behavior. While consensus has been established that the concentration of hydronium cations is enhanced at the surface with respect to the bulk, the affinity of hydroxide anions for the water/vapor interface has been a subject of an ongoing controversy. On the one hand, electrophoretic and titration measurements of air bubbles or oil droplets in water have been interpreted in terms of a dramatic interfacial accumulation of OH^-. On the other hand, surface-selective non-linear spectroscopies, surface tension measurements, and molecular simulations show no or at most a weak surface affinity of hydroxide ions. Here, we summarize the current situation and provide new evidence for the lack of appreciable surface enhancement of OH^-, based on photoelectron spectroscopy from a liquid jet and on molecular dynamics simulations with polarizable potentials at varying hydroxide concentrations.

*To whom correspondence should be addressed. E-mails: bernd.winter@bessy.de (B.W.) and pavel.jungwirth@uochb.cas.cz (P.J.).

1. Introduction and Historical Overview

Whether water's intrinsic anion, OH^-, strongly adsorbs at the water/vapor interface or not has led to a remarkable controversy in the scientific community recently. Interestingly, the contrasting view emerges primarily from macroscopic versus microscopic (molecular) approaches. The story starts already around the end of the 19th century, when accumulation of negative charge on small water droplets in nature has been described as the waterfall effect [1]. Similarly, charging upon aerodynamic breakup of water droplets has been first observed around the same time and has been revisited recently with the conclusion that the outermost layers of these droplets are negatively charged [2]. Electrophoretic measurements show that gas bubbles in water move toward the anode [3]. In distilled water this leads to a zeta-potential of about -35 mV, which can be titrated and changes sign around pH = 4 [3]. Similar behavior has been also observed for oil droplets in water [4-6]. Using titration measurements, it was derived that the charge adsorbed at the oil/water interface amounts to at least -5 $\mu C/cm^2$, i.e., one negative elementary charge per roughly 3 nm^2 [6, 7]. Adsorption of negative charge at aqueous hydrophobic interfaces was also invoked in measurements of disjoining pressure of thin aqueous films [8, 9].

In most of the above experiments the surface adsorbed negative charge has been interpreted in terms of hydroxide anions. A noticeble exception within macroscopic experiments is represented by surface tension measurements. Namely, surface tension of aqueous solutions of alkali hydroxides exhibits an increase (rather then a decrease, as is the case for strongly surface active species) with concentration [10]. Via direct application of the Gibbs adsorption equation [11] this leads to a conclusion that there is a net negative surface excess, i.e., a deficit of hydroxide in the interfacial layer of water. It is fair to say that, since surface excess is an integrated quantity over the whole interface, the increase in surface tension with concentration could be consistent with a modest surface enhancement of the host species provided it is overcompensated by subsurface depletion [12]. However, to

overcompensate the derived interfacial charge of hydroxide of -5 $\mu C/cm^2$ [7] would require a rather unrealistically thick layer of several milimeters completely devoid of OH^- [13].

Molecular calculations of hydroxide at the interface between water and vapor have been performed both in clusters and extended slabs employing empirical potentials or ab initio methods. Clusters exhibit a systematic shift from surface positions of hydroxide to its distribution over the whole volume upon increasing the number of water molecules [14-16]. Classical molecular dynamics (MD) simulations with polarizable potentials show that this trend projects to extended systems and that OH^- can be found almost equally distributed within aqueous slabs. More precisely, while hydroxide can penetrate all the way to the surface, on average it is found to be weakly (i.e., less than the alkali cation counterions) repelled from the top layer [17-19]. In contrast, for hydronium computational methods ranging from classical MD [14, 17, 20-22], over generalized valence bond simulations [23-25], to ab initio structural [26] and MD [18, 27] calculations show a relatively strong enhancement of water's intrinsic cation at the aqueous surface. With respect to the calculated surface excess of hydronium over hydroxide we have as a simple shortcut (i.e., ignoring ion activity issues) termed water surface as "acidic" [18].

Most recent ab initio MD simulations support the picture of OH^- not having any special surface binding sites [13], being at best very weakly attracted to water surface [28]. This view of water surface is also consistent with results of non-linear surface-selective spectroscopic measurements, i.e., Second Harmonic Generation (SHG) [29-31] and Vibrational Sum Frequency Generation (VSFG) [17, 32-34]. Similar behavior was observed also for soft hydrophobic (e.g., oil/water) interfaces, however, in contrast to the free water surface, hydroxide was found to exhibit a certain affinity for stiff hydrophobic interfaces, such as that between water and graphene [35-38]. Nevertheless, in these cases calculations show a surface propensity of hydronium as well, being actually stronger than that of hydroxide for a rigid hydrophobic wall [38].

In this paper, we provide new experimental and computational evidence for the lack of significant adsorption of hydroxide at the water/vapor interface. On the experimental side, we present synchrotron photoelectron spectroscopy (PES) measurements of NaOH in aqueous microjets in a broad concentration range from 0.1 to 3 M. This is the first time the behavior of hydroxide at the water/vapor interface has been addressed by a *linear* surface selective spectroscopic technique. These experiments are complemented by MD simulations of aqueous slabs containing NaOH in the corresponding concentration range. The present simulations employ a polarizable force field for water and ions which has been benchmarked against structural data from X-ray scattering recently [39]. Convoluting the calculated density profiles with the electron inelastic mean free path (IMFP) allows for a direct comparison to the measurements. Both MD simulations and PES experiments show a linear dependence of the interfacial OH^- signal on its bulk concentrations, which excludes strong surface accumulation of hydroxide. We discuss in detail the present results both in the light of previous supporting, as well as contradicting experiments.

2. Methods

2.1 Experimental

Photoemission studies of liquid water and NaOH aqueous solutions were performed at the U41 PGM undulator beamline of BESSY, Berlin, using a 15 μm vacuum liquid jet with a velocity of 120 m/s at 4 ^{o}C. At these experimental conditions photoelectrons ejected from the liquid phase travel a sufficiently long distance of several mm, reaching thus the electron analyzer without collisions with water vapor molecules. Details of the technique and of the experimental setup have been described elsewhere [40]. Briefly, photoexcitation is carried out with the synchrotron light polarization vector parallel to the flow of the liquid jet, with electron detection being normal to the polarization vector. The small focal size (23x12 μm^2) of the U41 PGM beamline, which provids photon energies in the 180-1400 eV range, allows

for a good matching of spatial overlaps between the synchrotron-light beam and the liquid jet. At typical jet operation conditions the pressure in the interaction chamber is in the upper 10^{-5} mbar range. The total experimental resolution was better than 250 meV at the electron-analyzer pass energy of 20 eV. Typical count rates were $>10^3$ per second. Highly demineralized water was used to prepare the solutions, and NaOH was of highest purity commercially available. A schematic picture of the interaction chamber together with a photograph of the frozen filaments from the liquid jet, collected at the liquid nitrogen cooled trap, are depicted in Figure 1.

2.2 Computational

Molecular dynamics simulations were performed in the geometry of an aqueous slab containing ~1500 water molecules in a prismatic unit cell of dimensions 2.87 x 2.87 x 28.7 nm. Applying 3D periodic boundary conditions, such a setup yielded an infinite set of mutually practically non-interacting extended slabs; each of them possessing an aqueous bulk region inbetween two solution/vapour interfaces [12]. A broad range of concentrations of NaOH were studied. In particular, we simulated the the following four aqueous NaOH solutions: 0.035, 0.49, 0.99, and 2.07 M, which were prepared by adding the corresponding number of Na^+ and OH^- ions to the water slab. Production runs of 20 ns (with the exception of the system with the lowest concentration of NaOH where 50 ns were necessary for providing acceptable statistics) were performed with a time step of 1 fs at constant volume and temperature (300 K), the latter being imposed via the Berendsen coupling [41].

All simulations were performed with a polarizable force field for water (POL3 [42]) and ions [19], which we successfully benchmarked against experimental bulk structural data [39] and ab initio calculations of small ion-water clusters [19] recently. Intramolecular interaction were cut off at 1.1 nm, with long range electrostatics being accounted for using the

Particle Mesh Ewald (PME) method [43]. All simulations were performed employing the program package Gromacs (version 3.3.1) compiled in double precision [44].

3. Results

3.1 Experimental

The oxygen 2pπ valence (i.e., from the highest occupied molecular orbital - HOMO), as well as the oxygen 1s core-level photoelectron spectra of NaOH aqueous solutions were measured for concentrations between 0.1 and 3.0m. Valence photoelectron (PE) spectra were obtained at photon energy of 200 eV, whereas the O1s core spectra were measured at two photon energies of 600 and 1200 eV. At 600 eV the solution interface is probed, while at 1200 eV the probe volume extends into the bulk solution [45]. Valence spectra at NaOH concentrations of 0.1, 0.2, 0.5, 1.0, and 2.0m, are shown in Figure 2. Here, electron binding energies (BE) are referenced using the well established $H_2O(aq)$ $1b_1$ photoelectron peak (11.16 eV [46]), and spectral intensities are normalized at the background signal near 40 eV BE. When measuring concentrations lower than ~0.05m the jet charges at the high photon fluxes used here, which would make the analysis of such data uncertain. In order to highlight the spectral changes as a function of OH^- concentration each trace of Figure 2 has, therefore, been overlaid with a reference spectrum of a 0.05m NaF aqueous solution - representing pure water in terms of hydroxide concentration. Fluoride salt was chosen because the lowest ionization energy of the solution, corresponding to removal of an $F^-(aq)$ 2p electron, is considerably higher than that of $OH^-(aq)$. Consequently, spectral overlap at the OH-(aq) lowest ionization energy of approximately 9.2 eV for 2pπ is avoided.

Our setup allows for an accurate determination of hydroxide intensities, even at the lowest concentrations used here. Other than the intensity changes of the OH- 2pπ peak, the solution and water spectra are almost identical. The only other noticeable difference is a peak at 35.4 eV BE which arises from direct $Na^+(aq)$ 2p photoelectrons [47]. As expected for the

small sodium cation with vanishing polarizability and, therefore, no surface enhancement [12], the Na-peak intensity increases linearly with concentration and can be used to double-check the nominal solution concentrations. More precisely, sodium is depleted from the top layer [12], however, unlike surface accumulation, depletion from the top water layer affects only very weakly the concentration dependence of the surface selective spectroscopic signal [31]. Since PES is a linear surface sensitive spectroscopy the OH^- signal evolution is a direct measure of the number increase of OH^- molecules in the probe volume. At the applied photon energy of 200 eV, the photoelectron kinetic energy (eKE) is approximately 190 eV, which roughly corresponds to a minimum of the electron IMFP curve [40]. Although the electron IMFP in water as a function of eKE still awaits accurate experimental determination, it is estimated that at 190 eV the top 1-3 layers of water are probed at most [45, 48].

The inset of Figure 2 is a zoom into the OH^-(aq) 2pπ peak-region for 0 - 3m NaOH aqueous solutions. From fitting each spectrum by two Gaussians, one for the water $1b_1$ peak, and the other for the OH^- 2pπ peak the respective peak intensities have been determined. The main result from this systematic study is the almost perfectly linear dependence of the valence OH^-(aq) 2pπ signal on bulk NaOH concentration, as depicted in Figure 3 (full circles). Note that in fitting the water $1b_1$ peak we have used for all concentrations the same parameters as obtained for water without any NaOH added [46]. Gaussian peaks for fitting the hydroxide component have been found to slightly depend on concentration. For 0.1m the OH^-(aq) 2pπ BE is 8.8 eV with 1.3 eV fwhm, while for 0.2m the BE is 9.0 eV with 1.6 eV fwhm. No further change in the peak width is observed up to the highest concentration but BEs further increase to 9.2 eV for concentrations above 1.5m.

The oxygen 1s PES measurements were performed for identical solutions as those used for the above valence studies. As shown in Figure 4 presenting the O1s PE spectra from 0.1, 1.0, and 2.0m NaOH aqueous solutions measured at 600 eV photon energy, the core-level spectra show distinct O1s contributions from H_2O(aq) and OH^-(aq), too. The former is the

main water peak (at 538.1 eV BE), while the latter gives rise to the low-energy shoulder (at 536.0 eV BE). The detailed intensity evolution of the OH^-(aq) peak as a function of concentration is shown in the inset of Figure 4. At the photon energy of 600 eV the O1s photoelectrons have approximately 60 eV KE, therefore, roughly the same depth is probed as in the valence case of Figure 2 [45]. The OH^- signal analysis was again based on peak fitting, where the use of three Gaussians for H_2O(g), H_2O(aq), and OH^-(aq) resulted in very good fits of the total experimental spectrum. As before, constant peak position and width for the water feature were assumed. Similarly to the valence data, the resulting OH^-(aq) O1s peak positions and widths were observed to slightly depend on concentration; 535.52 eV BE and 1.2 eV fwhm for 0.2m, 535.57 eV/1.2 eV (0.5m), 536.66 eV/1.2 eV (0.8m), 535.73 eV/1.2 eV (1.0m), 535.82 eV/1.4 eV (1.5m), 535.85 eV/1.4 eV (2.0m), and 536.00 eV/1.4 eV (3.0m). OH^-(aq) intensities were determined with respect to the normalized water PE signal, with the small solute volume effect on water density taken into account. The fitted OH^-(aq) O1s signal intensity as a function of concentration is shown in Figure 3 (full squares) along with the OH^-(aq) 2pπ results. It is reassuring that both sets of data reveal the same linear behavior.

In addition to collecting O1s spectra of the NaOH solutions at 600 eV photon energy, measurements were also performed at 1200 eV (Figure 5). In the latter case the probing depth is increased, extending to several nanometers [45, 48]. All spectra in Figure 5 have been normalized to the H_2O(aq) intensity at the main water peak at 538.1 eV BE, which explains the smaller gas-to-liquid phase ratio at 1200 eV due to larger probing depth and hence larger absolute H_2O(aq) signal. Unfortunately, a fully quantitative analysis of these spectra, that would deliver reliable OH^- intensities as a function of concentration, is not feasible since even the O1s PE spectrum of neat water exhibits a small peak at 536 eV at 1200 eV (which is absent at the 600 eV photon energy) [45]. Hence, the signal intensity differences that one observes at 536 eV BE for 600 vs 1200 eV excitation energy cannot be attributed to OH^- only.

At the present moment we are thus unable at 1200 eV to accurately distinguish between spectral contributions from a certain class of H_2O(aq) hydration configurations [45] and from OH^-(aq). Despite this problem, it is instructive to semi-quantitatively compare the PE signal differences between shallow and deeper probes at different concentrations. While trace *a)* in Figure 5 makes this comparison for the 0.2m NaOH aqueous solution, trace *b)* contrasts the spectra for 600 and 1200 eV photon energy for the 2.0m solution. The difference between 1200 and 600 eV excitation energy spectra at 536 eV BE at 0.2m NaOH is primarily due to the signal from bulk water molecules given the low concentration of the solute. This difference becomes larger for higher concentration (trace *b)* in Figure 5), which points to a contribution from OH^- at 2m. The fact that the signal at 536 eV BE is larger for 1200 eV which probes rather deep into the solution than at 600 eV (where the signal comes from the top few layers) thus seems to imply that there is more hydroxide in the bulk than at the surface.

3.2 Computational

The principal outputs from the present MD simulations are ion density profiles, i.e., histogramed populations of OH^- and Na^+ across the aqueous slab, averaged over the dimensions parallel to the surfaces and over the whole trajectory. Such density profiles, symmetrized over the two equivalent halves of the slabs, are presented for the four investigated sodium hydroxide concentrations of 0.035, 0.49, 0.99, and 2.07 M in Figure 6. We also display the density profile of the whole system, which defines a bulk region with a roughly constant density, an interfacial region with a sharp drop of density within ~0.4 nm, and vapor with just a handful of free water molecules and, correspondingly, vanishing density. Note that for visual clarity all density profiles are normalized such that the integrated areas under all the curves are the same, with the system density at zero (i.e., in the center of the slab) being set to unity.

Figure 6 demonstrates that at all four concentrations the investigated ions are repelled from the solution/vapor interface. However, there is a small but significant difference between OH^- and Na^+ in that the former ion penetrates closer to the interface and can actually be found also right at the surface with hydrogen pointing into the gas phase. This effect is the strongest at the lowest concentration (Figure 6a). There, only one anion and one cation is present in the system and, consequently, the two ions behave largely independent of each other. At higher concentrations cation-anion correlations come increasingly into play (Figures 6bcd). As a result, the density profiles of OH^- and Na^+ tend to overlap more and the interfacial signal from hydroxide decreases. At the highest concentration, we start to see extensive ion pairing and even an onset of ion clustering. The latter causes some loss of ergodicity of the MD trajectory and also explains the occurence of a peak on both of the ion density profiles roughly half way from the center of the slab to the surface (Figure 6d).

In order to establish a direct link between MD simulations and results of PES experiments, the density profiles from Figure 6 have to be attenuated due to the finite inelastic mean free path of the photoelectrons in water. The IMFP is inversely proportional to the integrated particle density from an emission depth z to z_o and the simulated total photoelectron response *I* from a species *A*, can be expressed as [48]

$$I \sim \int \rho_A(z)/\rho_0 \times \exp\left(-1/\mathrm{IMFP} \times \int \rho_{tot}(z)/\rho_0 \, dy\right) dz \qquad (1)$$

The function $\rho_A(z)$ describes the density profile of a species *A*, i.e., OH^- in the present simulations. $\rho_{tot}(z)$ is the calculated density profile of the whole system and ρ_o is the average total density in the bulk. Note that integration runs from the vapor across the interface deep into the aqueous phase. In calculations according to Eq. 1 we fixed ρ_o as the density of the whole system at zero, i.e., in the center of the slab, and assumed $\rho_A(z)$ and $\rho_{tot}(z)$ being constant at depths larger than that of the slab center.

As mentioned in the above section, in water the dependence of IMFP on eEK is not known precisely yet, however, for the present 600 eV photon energy experiments it can be estimated to be at least 0.5 - 1 nm. We have used these two values of IMFP in Eq. 1 to convert the density profiles from Figure 6 into the dependence of the simulated photoelectron response on the concentration of NaOH. The result, which is presented in Figure 7, shows an almost perfectly linear dependence of the simulated photoelectron signal from hydroxide on the NaOH concentration for both considered values of IMFP, in accord with the experimental observation (Figure 3). Note that assuming larger IMFPs (i.e., probing deeper into the bulk) can only make the dependence more linear.

4. Discussion

Analysis of the photoelectron spetra of NaOH aqueous solutions, collected from the topmost layers of the solutions, reveals a linear dependence of the OH^- density on bulk concentration over the entire range studied here (Figure 3). This finding is obtained for two independent experimental probes, the OH^-(aq) 2pπ valence electron signal and the OH^-(aq) O1s core electron signal. Since PES is a linear spectroscopy these results imply within the resolution of the experiment identical surface and bulk concentrations of hydroxide. To be more specific, strong surface accumulation of OH^- can be ruled out, as was also demonstrated by a fit to non-linear SHG spectroscopy data for surfaces of aqueous NaOH fitted to the Langmuir isotherm model [31]. What remains to be clarified is whether hydroxide is or is not repelled from the surface. In terms of distinguishing between zero and weak repulsion of OH^- from the surface experiments are, however, not very sensitive [31]. Nevertheless presents comparison between O1s PES at 600 and 1200 eV photon energies seems to point to the latter. Consistently with the measurements, the present MD simulations give an almost perfectly linear depedence of the calculated photoelectron signal on OH^- concentration, showing at the same time a weak surface repulsion of hydroxide from the surface.

Spectroscopic experiments and molecular simulations usually employ relatively concentrated solutions (typically >0.1 M, with SHG being able to go to ~10^{-3} M [31]), which calls for justification of validity of extrapolating to lower concentrations and to neat water. An argument in favor of such extrapolation is the strictly *linear* behavior over a broad concentration range from 0.1 to several moles of NaOH. In the same spirit, results of present simulations performed in what is sometimes called the "infinite dilution" limit with a single hydroxide anion in an extended aqueous slab are consistent with the interfacial behavior of OH^- in more concentrated solutions. The present results thus indicate an interfacial behavior of hydroxide that does not qualitatively change with concentration.

The relatively simple polarizable potential employed in the simulations in order to acheive satisfactory statistics for a sufficiently large system size may be a source of inaccuracies. The present empirical force field cannot capture dynamical effect connected with proton hopping in hydroxide solutions [49] and, consequently, the unusually high mobility of OH^- in water. Moreover, even the best empirical polarizable potential available can only approximately describe the subtleties of the immediate solvation shell around OH^- including charge delocalization. Nevertheless, the present force field benchamarks very well against accurate ab initio calculations on small clusters [19] and X-ray diffraction experiments in the aqueous bulk [39]. The surface behavior of OH^- observed in our classical MD simulations is also consistent with results from ab initio MD simulations, showing that hydroxide does not have any strong surface binding sites [13] and is at most very weakly (by less than kT) attracted to water surface [28].

The above microscopic experimental and computational results contradict the interpretation of several types of macroscopic experiments, from charging during aerodynamic breakup over electrophoretic mobilities of air bubbles and oil droplets to disjoining pressure measurements [2-5, 7-9]. These observations of a negative surface charge are well established, nevertheless, several problems arrise when comparing with microscopic

approaches. First, the exact location of the charged layer is not very well established in macroscopic measurements. In principle, it cannot be excluded that the charged layer lies deeper in the liquid than what is probed in surface selective spectroscopies or simulations, although it is difficult to imagine a force which would accumulate a significant amount of charge several nanometers or more from the surface. Second, macroscopic approaches do not directly reveal the chemical nature of the interfacial negative charge, although they do show that it is titratable [3-5]. Note that the interfacial charge of neat water of more than -5 $\mu C/cm^2$, i.e., one negative charge per ~3 nm^2 [6, 7] should be clearly detectable as an OH^- peak in the present PES experiment (but we do not see hydroxide in a NaOH-free jet) unless it is burried several nanometers below the surface or carried by a different species than hydroxide. Moreover, no matter where such a large interfacial charge would be located, if it were OH^- a strong negative change in surface tension with pH around neutrality should arise. This is, however, not observed [10, 13].

Conclusion

We have reviewed the present controversy concerning the surface behavior of hydroxide ions in water, addressing the disagreement between macroscopic experiments (except for surface tension measurements) and molecular scale experiments and simulations on whether OH^- does or does not strongly adsorb at the water/vapor interface. We have also performed new experiments and calculations aiming at resolving this issue. To this end, we have probed surfaces of aqueous solutions of NaOH in a broad concentration range by photoelectron spectroscopy and molecular dynamics simulations.

The present experiments and simulations provide a mutually consistent picture of the interfacial behavior of hydroxide. Synchrotron PES from aqueous microjets reveals a linear dependence of the interfacial OH^- signal on bulk NaOH concentration for two independent probes – oxygen valence $2p\pi$ and core 1s photoelectrons. This observation excludes strong

adsorption of hydroxide anions within the topmost layers of water. If anything, comparison between photoemission signals probing at different depths points to a weak repulsion of hydroxide from the surface.

Calculated photoemission intensities from OH^-, using density profiles from molecular dynamics simulations of aqueous solutions in extended slab geometry attenuated by the electron inelastic mean free path, also exhibit a linear dependence on bulk NaOH concentration. The result of calculations, i.e., that OH^- is weakly repelled or at best very weakly attracted to the surface, is thus in accord with the present linear PES experiment, as well as with previous non-linear spectroscopic measurements. This result is also in agreement with surface tension measurements. The disagreement with other macroscopic experiments, such as electrophoretic mobilities, titration, and disjoining pressure measurements can at least partially be tracked back to ambiguities in determining the accurate location and chemical nature of the interfacial negative charge observed using probes lacking molecular resolution.

Acknowledgment

We are grateful to the Czech Ministry of Education (grant LC512) and the Czech Science Foundation (grant 203/08/0114) for support. Part of the work in Prague was supported via Project Z40550506. R.V. acknowledges support from the International Max-Planck Research School. B.W. thanks the Deutsche Forschungsgemeinschaft (Project WI 1327/3-1) for support.

Figure captions

Figure 1 A photograph (a) and a schematic picture (b) of the experimental setup for synchotron photoelectron spectroscopy in aqueous microjets.

Figure 2 Valence photoelectron spectra of NaOH aqueous solutions from 0 to 3m. The photon energy was 200 eV. The reference water spectrum is overlaid for comparison in each trace. H_2O(aq) $2a_1$, $1b_2$, $3a_1$, and $1b_1$ emission is labeled. Inset: Enlargement of the spectral region from -10 to -6 eV BE for the OH^-(aq) $2p\pi$ peak for all investigated concentrations.

Figure 3 OH^-(aq) $2p\pi$, i.e., HOMO (circles) and OH^-(aq) oxygen 1s (squares) photoelectron signal as a function of OH^- concentration. Error bars connected with the analysis of the PE signal are approximately of the size of the symbols used in the figure. The line is a linear fit with correlation coefficient of 0.9975.

Figure 4 Oxygen 1s PE spectra of NaOH aqueous solutions for different concentrations, 0.2-2.0 molal. The photon energy was 600 eV. Spectral contributions from H_2O(gas), H_2O(aq), and OH^-(aq) are labeled. Inset: Zoom into the OH^-(aq) $2p\pi$ spectral region for all concentrations measured.

Figure 5 Comparison of the 0.2 and 2.0m oxygen 1s NaOH solution spectra, each measured at 600 and 1200 eV photon energy. Photoemission intensities are normalized to full scale.

Figure 6 Density profiles of OH^-, Na^+, and the whole system from the vapor across the solution/vapor interface into the aqueous bulk calculated for slabs with a) 0.035, b) 0.49, c) 0.99, and d) 2.07 M NaOH.

Figure 7 Simulated photoelectron signal from OH^- for two assumed values of the electron inelastic mean free path of 0.5 and 1.0 nm. Note the almost perfectly linear dependence of the signal on NaOH concentration, in accord with the experiment.

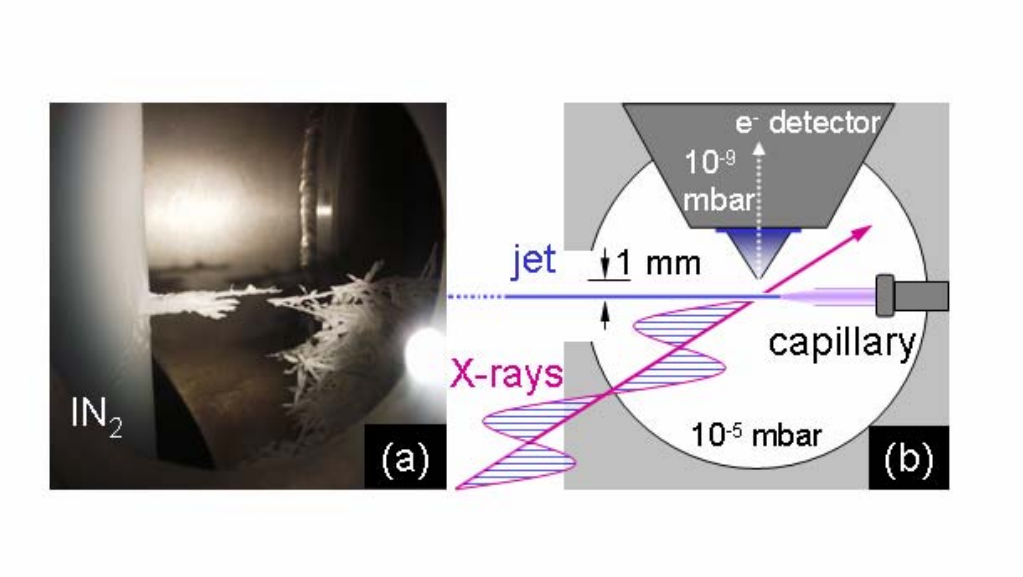

Figure 1

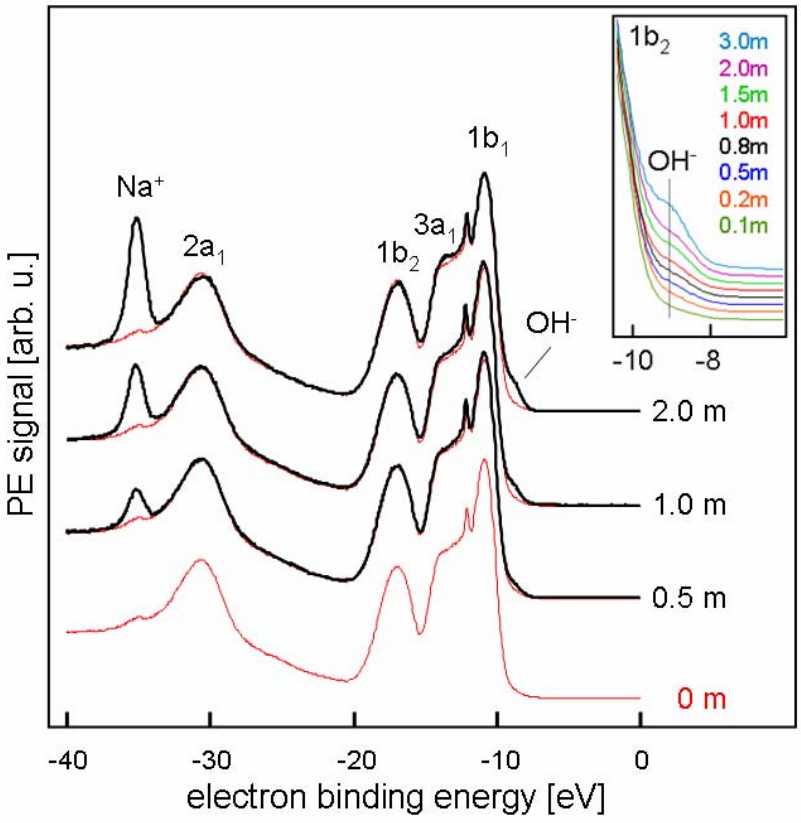
Na+
2a1
1b2
3a1
1b1
OH-
2.0 m
1.0 m
0.5 m
0 m
PE signal [arb. u.]
-40
-30
-20
-10
0
electron binding energy [eV]
1b2
OH-
3.0m
2.0m
1.5m
1.0m
0.8m
0.5m
0.2m
0.1m
-10
-8

Figure 2

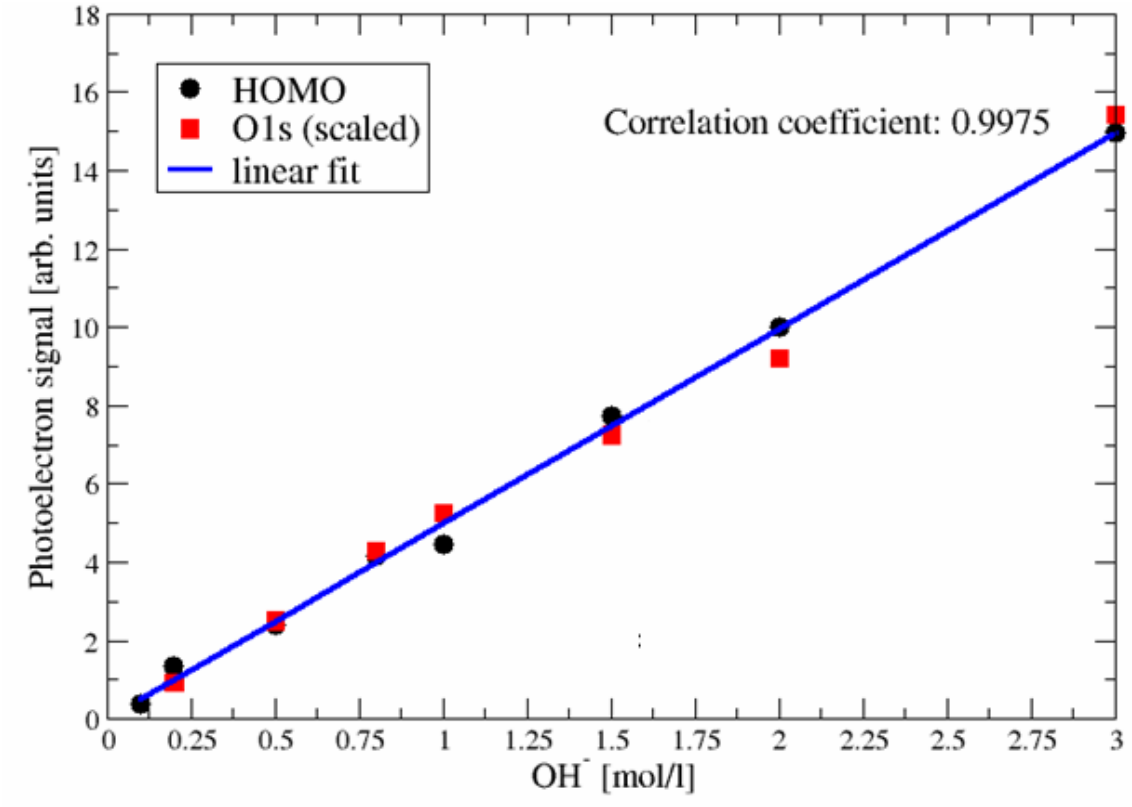
HOMO
O1s (scaled)
linear fit
Correlation coefficient: 0.9975
Photoelectron signal [arb. units]
OH⁻ [mol/l]
0
2
4
6
8
10
12
14
16
18
0
0.25
0.5
0.75
1
1.25
1.5
1.75
2
2.25
2.5
2.75
3

Figure 3

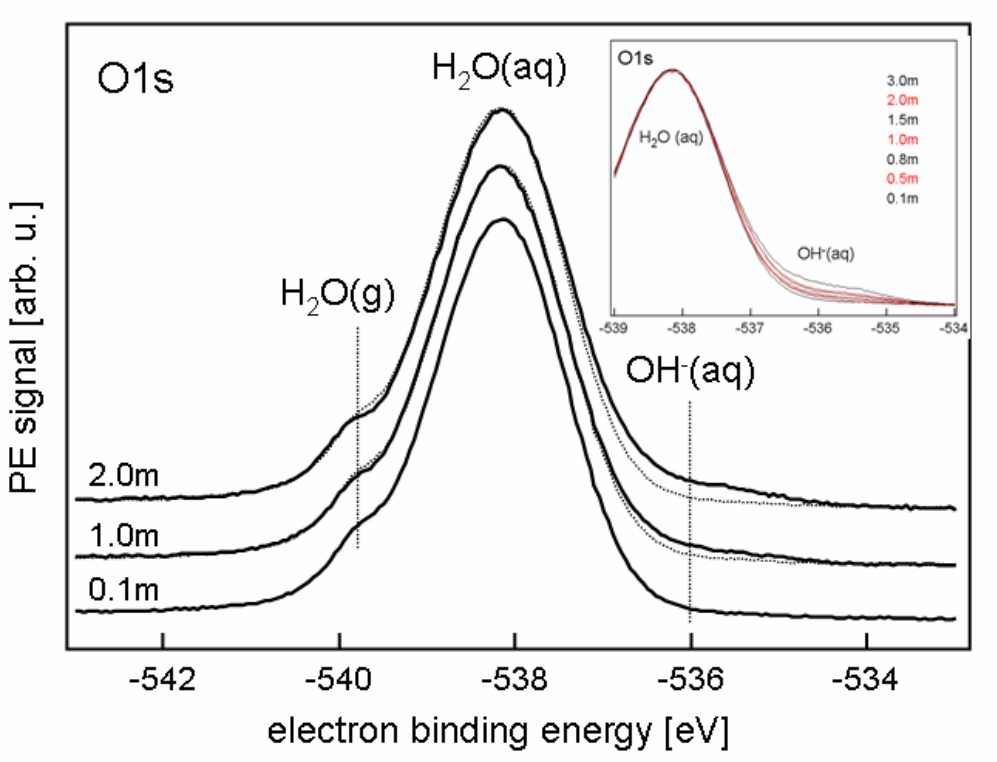
O1s
H2O(aq)
H2O(g)
OH-(aq)
2.0m
1.0m
0.1m
PE signal [arb. u.]
-542
-540
-538
-536
-534
electron binding energy [eV]
O1s
H2O (aq)
OH-(aq)
3.0m
2.0m
1.5m
1.0m
0.8m
0.5m
0.1m
-539
-538
-537
-536
-535
-534

Figure 4

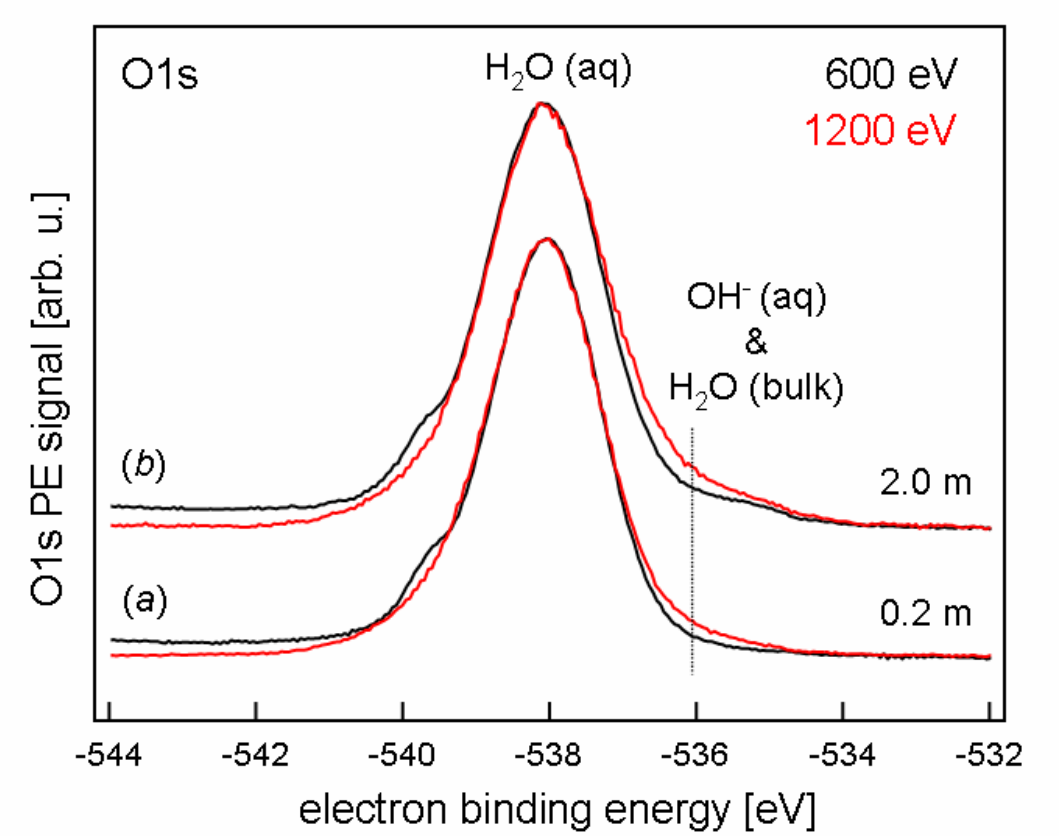
O1s
H2O (aq)
600 eV
1200 eV
OH- (aq)
&
H2O (bulk)
(b)
2.0 m
(a)
0.2 m
O1s PE signal [arb. u.]
-544
-542
-540
-538
-536
-534
-532
electron binding energy [eV]

Figure 5

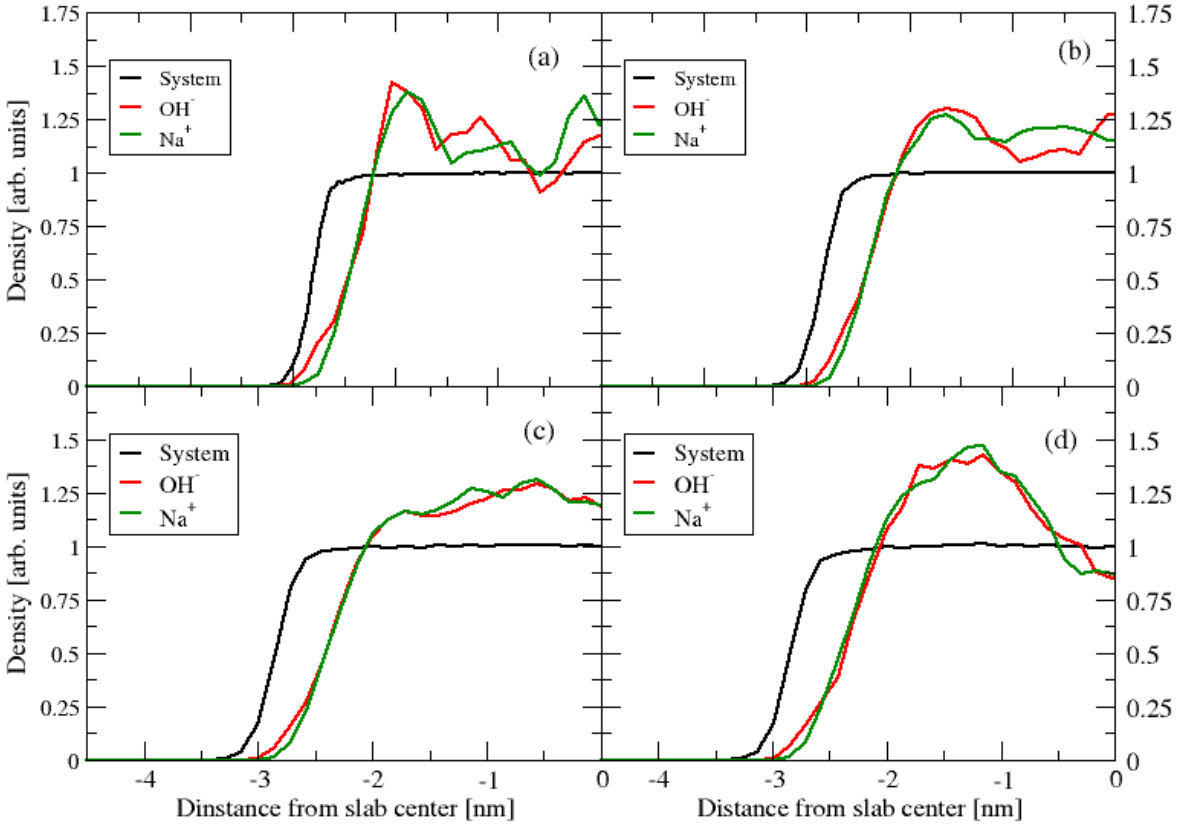
(a)
(b)
(c)
(d)
System
OH-
Na+
Density [arb. units]
Dinstance from slab center [nm]
Distance from slab center [nm]

Figure 6

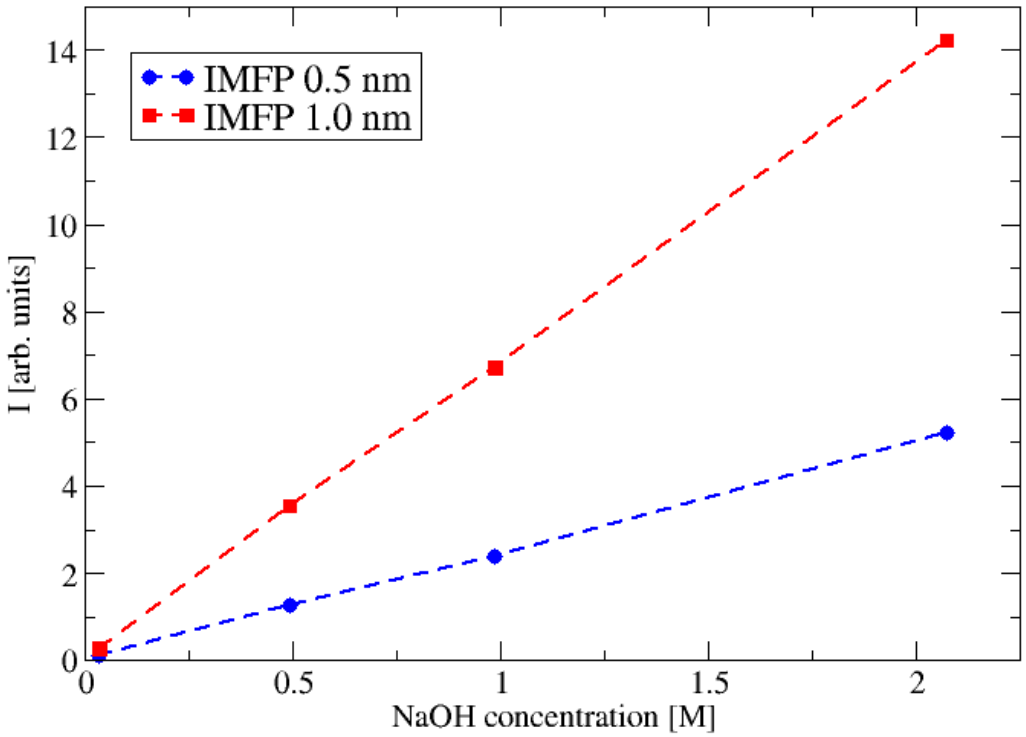
IMFP 0.5 nm
IMFP 1.0 nm
I [arb. units]
NaOH concentration [M]
0
2
4
6
8
10
12
14
0
0.5
1
1.5
2

Figure 7

References

1. Lenard, P., *Uber die Electricitat der Wasserfalle.* Ann. Physik., 1892. **46**: p. 584-636.
2. Zilch, L.W., J.T. Maze, J.W. Smith, G.E. Ewing, and M.F. Jarrold, *Charge Separation in the Aerodynamic Breakup of Micrometer-Sized Water Droplets.* Journal of Physical Chemistry A, 2008. **112**(51): p. 13352-13363.
3. Takahashi, M., *xi potential of microbubbles in aqueous solutions: Electrical properties of the gas-water interface.* Journal of Physical Chemistry B, 2005. **109**(46): p. 21858-21864.
4. Marinova, K.G., R.G. Alargova, N.D. Denkov, O.D. Velev, D.N. Petsev, I.B. Ivanov, and R.P. Borwankar, *Charging of oil-water interfaces due to spontaneous adsorption of hydroxyl ions.* Langmuir, 1996. **12**(8): p. 2045-2051.
5. Beattie, J.K. and A.M. Djerdjev, *The pristine oil/water interface: Surfactant-free hydroxide-charged emulsions.* Angewandte Chemie-International Edition, 2004. **43**(27): p. 3568-3571.
6. Beattie, J.K., A.M. Djerdjev, and G.G. Warr, *The surface of neat water is basic.* Faraday Discussion, 2009. **141**: p. 31-39.
7. Beattie, J.K., *The intrinsic charge on hydrophobic microfluidic substrates.* Lab on a Chip, 2006. **6**(11): p. 1409-1411.
8. Stubenrauch, C. and R. von Klitzing, *Disjoining pressure in thin liquid foam and emulsion films - new concepts and perspectives.* Journal of Physics-Condensed Matter, 2003. **15**(27): p. R1197-R1232.
9. Karraker, K.A. and C.J. Radke, *Disjoining pressures zeta potentials and surface tensions of aqueous non-ionic surfactant/electrolyte solutions: theory and comparison to experiment.* Advances in Colloid and Interface Science, 2002. **96**(1-3): p. 231-264.

10. Weissenborn, P.K. and R.J. Pugh, *Surface tension of aqueous solutions of electrolytes: Relationship with ion hydration, oxygen solubility, and bubble coalescence.* Journal of Colloid and Interface Science, 1996. **184**(2): p. 550-563.

11. Gibbs, J.W., *The Collected Works of J. Willard Gibbs*. 1928, New York: Longmans.

12. Jungwirth, P. and D.J. Tobias, *Specific ion effects at the air/water interface.* Chemical Reviews, 2006. **106**(4): p. 1259-1281.

13. Jungwirth, P., *Ions at Aqueous Interfaces.* Faraday Discussions, 2009. **141**: p. 9-30.

14. Brodskaya, E., A.P. Lyubartsev, and A. Laaksonen, *Investigation of water clusters containing OH- and H3O+ ions in atmospheric conditions. A molecular dynamics simulation study.* Journal of Physical Chemistry B, 2002. **106**(25): p. 6479-6487.

15. Vegiri, A. and S.V. Shevkunov, *Hydration shell structure of the OH-(H2O)(n=1-15) clusters from a model potential energy function.* Journal of Chemical Physics, 2000. **113**(19): p. 8521-8530.

16. Lee, H.M., P. Tarkeshwar, and K.S. Kim, *Structures, energetics, and spectra of hydrated hydroxide anion clusters.* Journal of Chemical Physics, 2004. **121**(10): p. 4657-4664.

17. Mucha, M., T. Frigato, L.M. Levering, H.C. Allen, D.J. Tobias, L.X. Dang, and P. Jungwirth, *Unified molecular picture of the surfaces of aqueous acid, base, and salt solutions.* Journal of Physical Chemistry B, 2005. **109**(16): p. 7617-7623.

18. Buch, V., A. Milet, R. Vacha, P. Jungwirth, and J.P. Devlin, *Water surface is acidic.* Proceedings of the National Academy of Sciences of the United States of America, 2007. **104**(18): p. 7342-7347.

19. Vacha, R., V. Buch, A. Milet, P. Devlin, and P. Jungwirth, *Autoionization at the surface of neat water: is the top layer pH neutral, basic, or acidic?* Physical Chemistry Chemical Physics, 2007. **9**: p. 4736-4747.

20. Kusaka, I. and D.W. Oxtoby, *Evaluating free energy, enthalpy, and entropy of protonated water clusters by a grand canonical Monte Carlo simulation.* Journal of Chemical Physics, 2000. **113**(22): p. 10100-10104.

21. Dang, L.X., *Solvation of the hydronium ion at the water liquid/vapor interface.* Journal of Chemical Physics, 2003. **119**(12): p. 6351-6353.

22. Ishiyama, T. and A. Morita, *Molecular dynamics analysis of interfacial structures and sum frequency generation spectra of aqueous hydrogen halide solutions.* Journal of Physical Chemistry A, 2007. **111**(38): p. 9277-9285.

23. Petersen, M.K., S.S. Iyengar, T.J.F. Day, and G.A. Voth, *The hydrated proton at the water liquid/vapor interface.* Journal of Physical Chemistry B, 2004. **108**(39): p. 14804-14806.

24. Iyengar, S.S., M.K. Petersen, T.J.F. Day, C.J. Burnham, V.E. Teige, and G.A. Voth, *The properties of ion-water clusters. I. The protonated 21-water cluster.* Journal of Chemical Physics, 2005. **123**(8).

25. Swanson, J.M.J., C.M. Maupin, H.N. Chen, M.K. Petersen, J.C. Xu, Y.J. Wu, and G.A. Voth, *Proton solvation and transport in aqueous and biomolecular systems: Insights from computer simulations.* Journal of Physical Chemistry B, 2007. **111**(17): p. 4300-4314.

26. Shin, J.W., N.I. Hammer, E.G. Diken, M.A. Johnson, R.S. Walters, T.D. Jaeger, M.A. Duncan, R.A. Christie, and K.D. Jordan, *Infrared signature of structures associated with the H+(H2O)(n) (n=6 to 27) clusters.* Science, 2004. **304**(5674): p. 1137-1140.

27. Iyengar, S.S., T.J.F. Day, and G.A. Voth, *On the amphiphilic behavior of the hydrated proton: an ab initio molecular dynamics study.* International Journal of Mass Spectrometry, 2005. **241**(2-3): p. 197-204.

28. Tobias, D.J., C.J. Mundy, M.E. Tuckerman, and L.X. Dang, private communication.

29. Petersen, P.B. and R.J. Saykally, *Evidence for an enhanced hydronium concentration at the liquid water surface.* Journal of Physical Chemistry B, 2005. **109**(16): p. 7976-7980.

30. Petersen, P.B. and R.J. Saykally, *On the nature of ions at the liquid water surface.* Annual Review of Physical Chemistry, 2006. **57**: p. 333-364.

31. Petersen, P.B. and R.J. Saykally, *Is the liquid water surface basic or acidic? Macroscopic vs. molecular-scale investigations.* Chemical Physics Letters, 2008. **458**(4-6): p. 255-261.

32. Schnitzer, C., S. Baldelli, and M.J. Shultz, *Sum frequency generation of water on NaCl, NaNO3, KHSO4, HCl, HNO3, and H2SO4 aqueous solutions.* Journal of Physical Chemistry B, 2000. **104**(3): p. 585-590.

33. Tarbuck, T.L., S.T. Ota, and G.L. Richmond, *Spectroscopic studies of solvated hydrogen and hydroxide ions at aqueous surfaces.* Journal of the American Chemical Society, 2006. **128**(45): p. 14519-14527.

34. Tian, C.S., N. Ji, G.A. Waychunas, and Y.R. Shen, *Interfacial structures of acidic and basic aqueous solutions.* Journal of the American Chemical Society, 2008. **130**(39): p. 13033-13039.

35. Zangi, R. and J. Engberts, *Physisorption of hydroxide ions from aqueous solution to a hydrophobic surface.* Journal of the American Chemical Society, 2005. **127**(7): p. 2272-2276.

36. Kudin, K.N. and R. Car, *Why are water-hydrophobic interfaces charged?* Journal of the American Chemical Society, 2008. **130**(12): p. 3915-3919.

37. Vacha, R., R. Zangi, J.B.F.N. Engberts, and P. Jungwirth, *Water structuring and hydroxide ion binding at the interface between water and hydrophobic walls of varying rigidity and van der waals interactions.* Journal of Physical Chemistry C, 2008. **112**(20): p. 7689-7692.

38. Vacha, R., D. Horinek, M.L. Berkowitz, and P. Jungwirth, *Hydronium and hydroxide at the interface between water and hydrophobic media.* Physical Chemistry Chemical Physics, 2008. **10**(32): p. 4975-4980.

39. Vacha, R., T. Megyes, I. Bako, L. Pusztai, and P. Jungwirth, *Benchmarking Polarizable Molecular Dynamics Simulations of Aqueous Sodium Hydroxide by Diffraction Measurements.* Journal of Physical Chemistry A, 2009: p. DOI: 10.1021/jp810399p

40. Winter, B. and M. Faubel, *Photoemission from liquid aqueous solutions.* Chemical Reviews, 2006. **106**(4): p. 1176-1211.

41. Berendsen, H.J.C., J.P.M. Postma, W.F. Vangunsteren, A. Dinola, and J.R. Haak, *Molecular-Dynamics with Coupling to an External Bath.* Journal of Chemical Physics, 1984. **81**(8): p. 3684-3690.

42. Caldwell, J.W. and P.A. Kollman, *Structure and Properties of Neat Liquids Using Nonadditive Molecular-Dynamics - Water, Methanol, and N-Methylacetamide.* Journal of Physical Chemistry, 1995. **99**(16): p. 6208-6219.

43. Essmann, U., L. Perera, M.L. Berkowitz, T. Darden, H. Lee, and L.G. Pedersen, *A Smooth Particle Mesh Ewald Method.* Journal of Chemical Physics, 1995. **103**(19): p. 8577-8593.

44. Lindahl, E., B. Hess, and D. van der Spoel, *GROMACS 3.0: a package for molecular simulation and trajectory analysis.* Journal of Molecular Modeling, 2001. **7**(8): p. 306-317.

45. Winter, B., E.F. Aziz, U. Hergenhahn, M. Faubel, and I.V. Hertel, *Hydrogen bonds in liquid water studied by photoelectron spectroscopy.* Journal of Chemical Physics, 2007. **126**.

46. Winter, B., R. Weber, W. Widdra, M. Dittmar, M. Faubel, and I.V. Hertel, *Full valence band photoemission from liquid water using EUV synchrotron radiation.* Journal of Physical Chemistry A, 2004. **108**(14): p. 2625-2632.

47. Weber, R., B. Winter, P.M. Schmidt, W. Widdra, I.V. Hertel, M. Dittmar, and M. Faubel, *Photoemission from aqueous alkali-metal-iodide salt solutions using EUV synchrotron radiation.* Journal of Physical Chemistry B, 2004. **108**(15): p. 4729-4736.

48. Ottosson, N., M. Faubel, S.E. Bradforth, P. Jungwirth, and B. Winter, *Photoelectron spectroscopy of liquid water and aqueous solution: Electron probing-depth and emission-angle anisotropy* Journal of Physical Chemistry B. **to be submitted**.

49. Tuckerman, M.E., A. Chandra, and D. Marx, *Structure and dynamics of OH-(aq).* Accounts of Chemical Research, 2006. **39**(2): p. 151-158.